02,08

Characteristics of YBCO|CeO$_2$|Al$_2$O$_3$ structures with decreasing thickness of the cerium oxide sublayer

© A.V. Boryakov, D.V. Masterov, S.A. Pavlov, A.E. Parafin¶, P.A. Yunin

Federal Research Center A.V. Gaponov-Grekhov Institute of Applied Physics of the Russian Academy of Sciences,
Nizhny Novgorod, Russia

¶ E-mail: parafin@ipmras.ru

The transport properties, surface morphology and structure of epitaxial $Y_1Ba_2Cu_3O_{7-x}$ (YBCO) films have been studied with decreasing thickness of the CeO_2 epitaxial buffer layer on sapphire. It has been shown that the critical temperature and critical current density of YBCO films retain high values ($T_c > 87$ K, $J_c(77$ K$) > 2$ MA/cm^2) as the thickness of the CeO_2 sublayer decreases from 100 nm to 1.2 nm. YBCO films remain superconducting on a CeO_2 layer with an equivalent thickness of 0.1 nm. The study was carried out with financial support of Russian Science Foundation as a part of scientific project no. 24-29-00824. The equipment of the Center for Collective Use of Institute for Physics of Microstructures of Russian Academy of Sciences "Physics and Technology of Micro- and Nanostructures" was used.

1. Introduction

Cryogenic electronics based on superconducting structures currently has a broad range of applications. This is attributable to the fact that the methods of studies and technology of manufacturing of structures based on films of high-temperature superconductor (HTSC) $Y_1Ba_2Cu_3O_{7-x}$ (YBCO) have reached a high level (see for instance, [1–5]). Voltage standards [2,3,6], THz signal generators [7,8], detectors [9–12], low-noise amplifiers and mixers [13,14] have been developed for various applications based on Josephson HTSC contacts. HTSC films are used in high-frequency devices due to the low surface resistance: resonators, filters [15] and detectors [16]. High-current electronics also use film HTSC current limiters [17].

However, the technological route for forming electronic circuits is as follows with all the variety of methods for application of YBCO films, performing optical or electronic lithography, as well as methods for etching YBCO films:

— deposition of YBCO film to the substrate;

— creation of a protective mask using optical or electronic lithography defining the topology of the circuit;

— YBCO etching [18,19] or ion implantation [20–22].

The etching or ion implantation operations used worsen the final parameters of the formed structures due to high sensitivity of the properties of YBCO films to external impacts.

We propose an alternative technological route using the following features of YBCO's growth on sapphire:

— YBCO films on sapphire with a sublayer of epitaxial cerium oxide (CeO$_2$) have high electrophysical characteristics [23,24];

— YBCO films deposited in the same modes on sapphire substrates (Al$_2$O$_3$) without a sublayer of CeO$_2$ are not superconducting.

The proposed sequence of operations is as follows:

— a protective mask of a given topology is formed from a photoresist or an electronic resist on a sapphire substrate with a solid sublayer of CeO$_2$;

— CeO$_2$ etching is performed to sapphire;

— YBCO is deposited in the epitaxial growth mode on the „islands" of CeO$_2$ on Al$_2$O$_3$ formed by etching.

As a result, superconducting circuit elements are formed on „islands" of CeO$_2$, and separating non-superconducting regions are formed between them, on the surface of the sapphire servicing as an insulator between superconducting elements. This sequence of operations actually substitutes the etching of the YBCO film by etching of the CeO$_2$ film. By forming the topology of the epitaxial cerium oxide circuit on a sapphire substrate, we obtain the topology of the superconducting circuit directly during the deposition of YBCO, without subsequent etching of the superconductor film.

It is important to note that the edges of superconducting elements are not degraded when the topology of the pattern is formed using this method unlike etching or ion implantation.

In practice, the sequence of technological operations may be somewhat more complicated: the topology of micron sized „islands" of CeO$_2$ will be created by optical lithography and ion etching; and electron-beam lithography together with ion etching or „cutting" of CeO$_2$ by a focused ion beam (FIB) will be used to form submicron circuit elements.

It is critically important to reduce the thickness of the CeO$_2$ film in this case. Reduction of the thickness of the

CeO_2 reduces the resistance requirements (i.e. thickness) of the resistive mask. In addition, the thinner the layer of CeO_2, the higher the accuracy of reproduction of the submicron dimensions of superconducting elements and the gaps between them, both during ion etching under the protection of a mask and when using FIB.

It is possible to formulate the task to be solved in this study based on the above: to determine the minimum thickness of the epitaxial cerium oxide layer on sapphire, which can be used to create a mask („islands" of CeO_2 on sapphire), defining the topology of superconducting structures with submicron sizes.

2. Structure formation technology

Monocrystalline sapphire substrates with orientation $(1\bar{1}02)$ (r-cut) were used in the study. Epitaxial cerium oxide (CeO_2) was deposited by laser sputtering, epitaxial film of YBCO was deposited by magnetron sputtering. The parameters of the technological processes and the sequence of operations used in this study to form the topology of the structures of YBCO bridges are described in detail in our article [25] (see „double-layer master mask" in it).

The substrate had a size of 10×10 mm. One half of the substrate was a continuous film, on which the structure of CeO_2 was studied by X-ray diffraction, and the structure of the YBCO film was studied after deposition of YBCO. The other half of the substrate comprise YBCO bridges of various widths (sizes on the photomask 1, 2, 4 and $10\,\mu$m, three bridges of each size) for measuring the superconducting characteristics of the YBCO film such as a critical current and critical temperature.

Contacts to the formed structures were made by thermal sputtering. Contact material is silver with thickness of $100-200$ nm.

3. Measurement procedures

The surface morphology of the structures was studied using scanning electron microscope CarlZeiss EVO 10 (secondary electron images). The electrical characteristics of the structures were measured by the four-probe method in a Dewar vessel with liquid nitrogen. The critical temperature T_c was determined by the zeroing of resistance of the superconducting bridge (current $100\,\mu$A, level $1\,\mu$V), the critical current of the bridge was measured at a temperature of 77 K at the level of $1\,\mu$V. The critical current density J_c was calculated using the values of the critical current, the width of the bridge and the thickness of the YBCO film. The width of the YBCO bridges was determined using the photographs taken by electronic scanning and optical microscopes. X-ray diffractometer BRUKER D8 DISCOVER was used to study of the structure and control the thickness of the layers of CeO_2 and YBCO. Additionally, the thickness of the layers was measured using the formed step in optical measuring system TALYSURF CCI 2000.

4. Determination of the thickness of the epitaxial layers of YBCO and CeO_2

The thicknesses of the epitaxial layers of YBCO and CeO_2 on sapphire substrates were determined using X-ray diffractometer BRUKER D8 DISCOVER by two methods: small-angle X-ray reflectivity (XRR) and X-ray diffractometry (XRD). Figure 1 shows the characteristic XRR curve for the double-layer structure of YBCO|CeO_2 on a sapphire substrate. The Kissing thickness oscillations are clearly visible for the thicker YBCO layer and the thin sublayer of CeO_2. The results of the experiment were processed in the DIFFRAC.Leptos software package by fitting a theoretical curve calculated based on a structure model that takes into account the density, thickness of layers and roughness of interfaces. The thickness of the YBCO layer was 84 nm, the thickness of the sublayer pf CeO_2 was 3.4 nm in the example shown in Figure 1 (sample MP2.270|L609). Additional thickness control was performed by X-ray diffractometry based on the period of thickness contrast oscillations near the diffraction peaks pf (005) YBCO and (002) CeO_2. The values obtained using various methods match with an accuracy of up to $1-2$ nm. The XRR method always provides higher values than XRD, since it is also sensitive to transition layers, unlike XRD, which determines the thickness of only as „good" for crystalline, „coherent" layer. The thickness of the CeO_2 on the sample L609, determined by X-ray diffractometry, was 3.4 nm, and the thickness defined by growth rate and number of pulses was 5 nm, which gives a deviation of 35%.

The correctness of determination of the thickness of CeO_2 was also verified using a sample L545 obtained by chemical etching of the structure of YBCO|CeO_2|Al_2O_3, on which, for some reason, part of CeO_2 separated from the substrate. As a result, the thickness of CeO_2 was measured on the resulting step by optical interferometry. The thickness of CeO_2 on the sample L545, defined by growth rate and the number of pulses is 56 nm, the thickness measured by X-ray
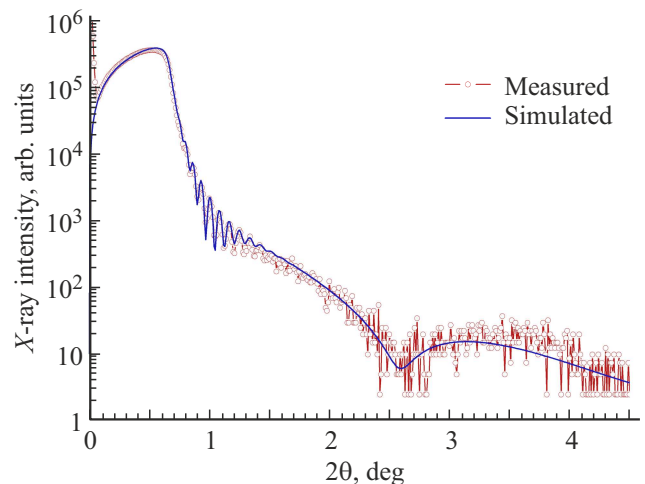
Figure 1. XRR curve of CeO_2 for a double-layer YBCO|CeO_2 structure on a sapphire substrate: experiment and model fitting.
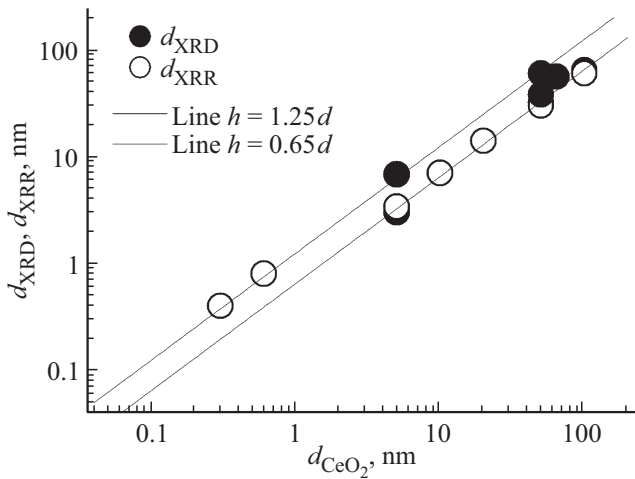
Figure 2. Results of measurements of the thickness of the epitaxial sublayer of cerium oxide d_{XRD} of CeO$_2$ and d_{XRR} of CeO$_2$ by X-ray diffraction methods (XRR and XRD, respectively). Straight lines show the maximum deviation of the measured thickness d_{XRD} of CeO$_2$ and d_{XRR} of CeO$_2$ from thickness d defined based on the number of pulses. Straight lines correspond to the maximum deviations of the thickness measured by XRD methods from the defined thickness: up — 25%; down — 35%.

diffraction is 70 nm. The height of the step of CeO$_2$|Al$_2$O$_3$ was 70 nm. Therefore, we obtained matching thickness values of 70 nm by of X-ray and interference measurements and this value is 25% greater than the thickness defined by the growth rate and the number of pulses.

The growth rate and position of the laser torch were checked before each cerium oxide deposition process. The cerium oxide was deposited for this purpose on a silicon substrate under the same technological conditions, only without heating the substrate. The thickness and position of the laser torch were controlled based on the location of the spot and the interferometric color on the substrate.

We further give the thickness d of layers of CeO$_2$, calculated based on the number of pulses during laser deposition and the known growth rate of CeO$_2$, which for „thick" layers of CeO$_2$ was 0.033 nm per pulse because, firstly, the measurements of the thickness of CeO$_2$ were performed not on all samples, and secondly, the minimum thickness of cerium oxide, which could be measured by X-ray diffraction, was 3.4 nm. We determined the deviation of the obtained thickness of CeO$_2$ from the thickness determined based on number of laser pulses as $+25-(-35)\%$ on an array of 12 samples (see Figure 2) by comparing the thicknesses of cerium oxide calculated based on the number of pulses and the growth rate, and the thicknesses measured by X-ray diffraction methods.

The thickness of the YBCO layer was determined based on the deposition time and was controlled by X-ray diffraction methods. The YBCO thickness was controlled on all samples, so we provide the thickness of the layers determined based on the deposition time and growth rate. An analysis of the differences of thicknesses defined

based on the deposition time and measured by X-ray diffraction methods allowed determining the deviation of the resulting YBCO thickness from the defined thickness as $+5-(-20)\%$.

5. Experimental results

22 structures of YBCO|CeO$_2$|Al$_2$O$_3$ were fabricated and measured for this study. The thicknesses of the CeO$_2$ layers defined based on the number of laser pulses ranged from 0.03 to 100 nm.

Figures 3 and 4 show the results of measurements of the electrophysical characteristics (J_c and T_c) of samples with YBCO layers formed on sublayers of various thicknesses. The critical current density slightly changes and retains high values $J_c > 2.7\,\mathrm{MA/cm^2}$ (77 K), characteristic of films on „thick" layer of CeO$_2$ when the thickness of the
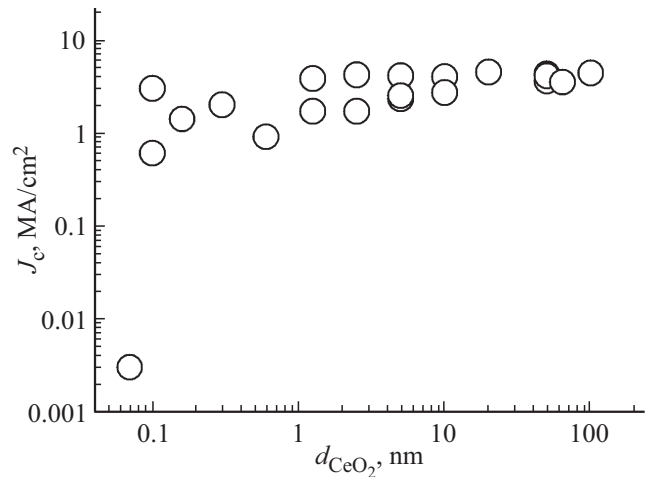
Figure 3. Dependence of the critical current density J_c of the YBCO film (at 77 K) on the thickness of the epitaxial sublayer of cerium oxide.
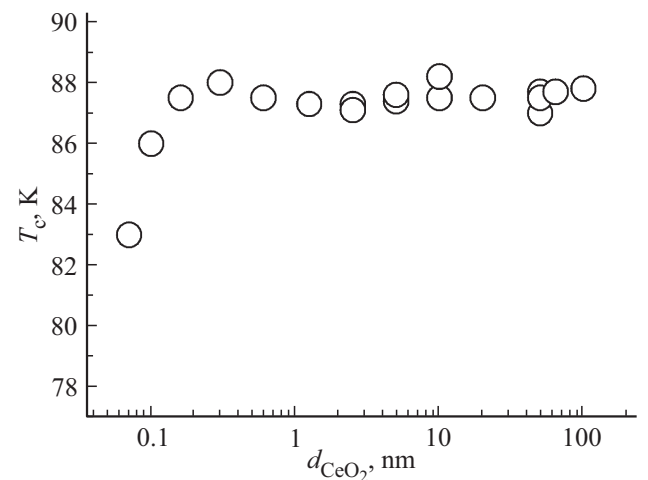
Figure 4. The dependence of the critical temperature T_c of the YBCO film on the thickness of the epitaxial sublayer of cerium oxide.
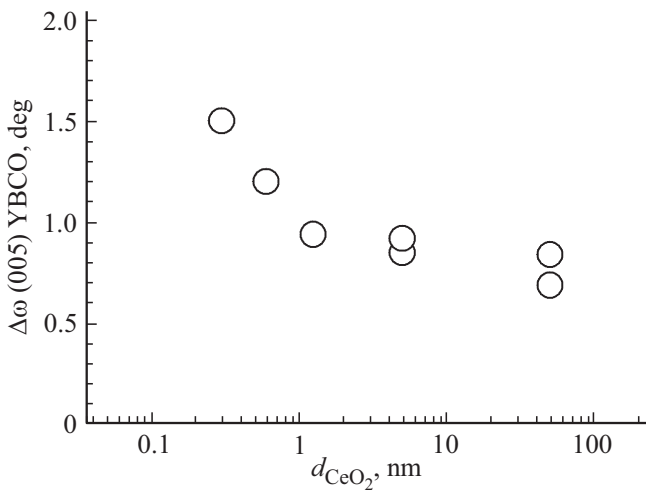
Figure 5. Disorientation of mosaic blocks ($\Delta\omega(005)$) of YBCO films depending on the thickness of the epitaxial sublayer of cerium oxide.
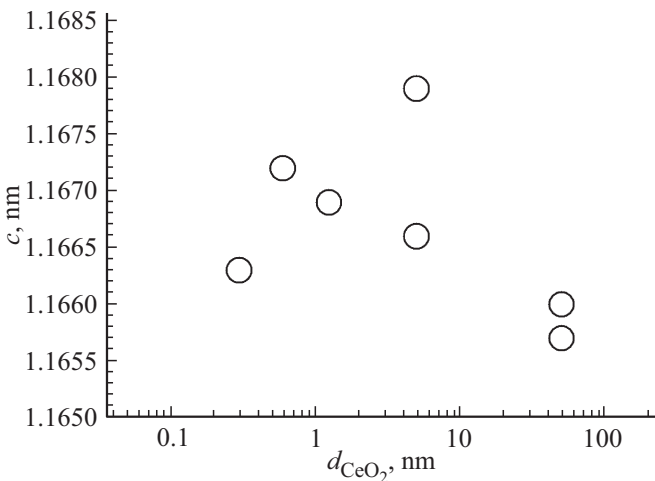
Figure 6. The value of the axis c of YBCO films depending on the thickness of the epitaxial sublayer of cerium oxide.

CeO$_2$ sublayer decreases to 1.2 nm. CeO$_2$ T_c also slightly varies in this range of layer thicknesses. J_c decreases to 0.6 MA/cm^2 and T_c decreases to 86 K in case of reduction of the equivalent thickness of the layer of CeO$_2$ to 0.1 nm. The transport characteristics of the YBCO film deteriorate with a further decrease of the thickness of the CeO$_2$ sublayer.

Figures 5 and 6 show the half-width of the swing curve $\Delta\omega(005)$ of YBCO, characterizing the disorientation of the mosaic blocks, and the magnitude of the axis with YBCO. The disorientation of the YBCO film mosaic blocks in the CeO$_2$ sublayer thickness range from 100 to 1.2 nm is 0.69−0.94°. The value of $\Delta\omega(005)$ of YBCO increases to 1.5° when the thickness of CeO$_2$ decreases to 0.3 nm. The measured value of the axis with YBCO up to the thickness of 0.3 nm of CeO$_2$ sublayer has a value corresponding to the optimal oxygen concentration in YBCO [26,27].

The given structural characteristics correspond to high-quality YBCO films.

Figures 7−9 shows secondary electrons images of the surface of structures MP2.269|L607, MP2.272|L612 and MP2.275|L622 with thicknesses of CeO$_2$ layers of 10, 1.25
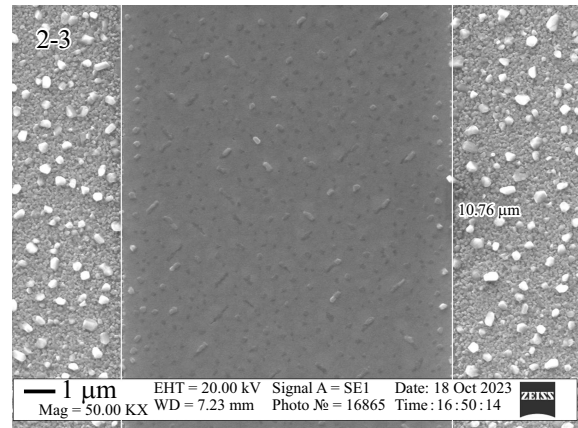
Figure 7. Image of the surface of the YBCO film of the MP2.269|L607 structure with a thickness of CeO$_2$ 10 nm.
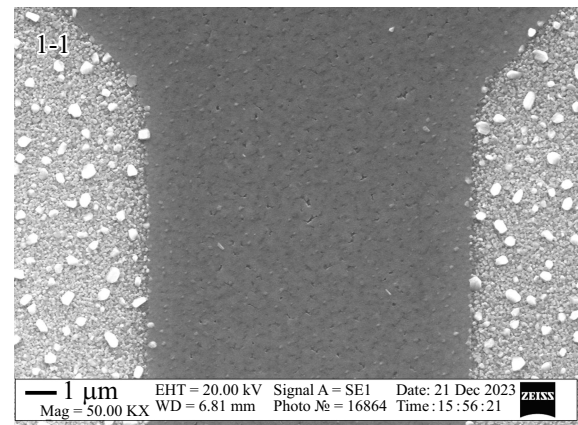
Figure 8. Image of the surface of the YBCO film of the MP2.272|L612 structure with a thickness of CeO$_2$ 1.25 nm.
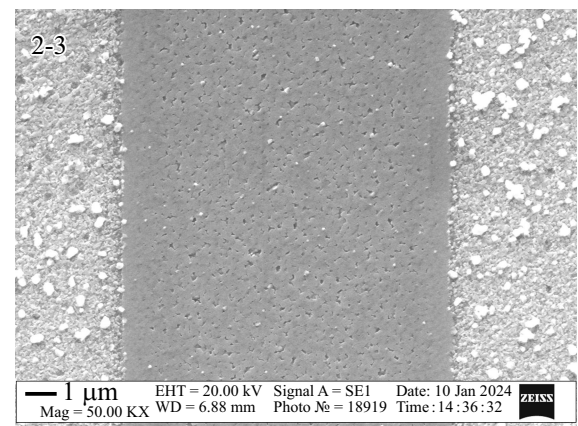
Figure 9. Image of the surface of the YBCO film of the MP2.275|L622 structure with a thickness of CeO$_2$ 0.3 nm.

and 0.3 nm, respectively. YBCO surface (bridge fragment with width of $10\,\mu$m) in the center (dark field), insulating separating area at the edges.

A comparison of the surface morphology of YBCO films grown on thin and ultrathin sublayers of CeO_2 shows their difference. This difference is attributable precisely to the peculiarities of YBCO growth on sublayers of different thicknesses, and not to a change, for example, of the cationic composition of HTSC, i.e., because the films were grown in the same growth modes. 10 nm CeO_2 film MP2.269|L607 (Figure 7), as well as films with higher thicknesses studied in this paper, has a characteristic appearance for films with high electrophysical characteristics of a YBCO matrix with inclusions of Y-enriched and Cu-enriched (outgrowths on the film surface) secondary phases with sizes of $\sim 0.5\,\mu$m and above. It can be seen that some of the precipitates have an elongated shape, and these particles are oriented along the substrate at right angles to each other. The visible dimensions of most of the precipitates are noticeably smaller on sample MP2.272|L612 1.25 nm CeO_2 (Figure 8) than on MP2.269|L607 10 nm CeO_2 — $0.1-0.2\,\mu$m. In this respect, the film looks smoother, however, pores and „gaps" of submicron sizes appear in the matrix. Gaps and pores in the matrix are the predominant type of defects in sample MP2.275|L622 0.3 nm CeO_2. The discontinuities retain submicron sizes but their density is significantly higher than in sample MP2.272|L612 1.25 nm CeO_2.

6. Conclusion

The morphology, critical temperature and critical current density of YBCO films grown on CeO_2|Al_2O_3 substrates weakly depend on the thickness of the epitaxial sublayer of CeO_2 in the range from 100 to 1.2 nm. Obtained characteristics of YBCO films: $T_c > 87$ K; $J_c(77\,\text{K}) > 2\,\text{MA/cm}^2$. The disorientation of the mosaic blocks of film YBCO $\Delta\omega(005)$ YBCO in the specified thickness range is $0.69-0.94°$. The transport and structural characteristics of YBCO deteriorate with a further decrease of the thickness of the CeO_2 sublayer. The films retain superconducting properties ($T_c > 83$ K) on the CeO_2 layer with an equivalent thickness of 0.1 nm. There are no fundamental changes in the morphology of YBCO films with a decrease of the thickness of the CeO_2 sublayer to nanometer values.

Consequently, the nanometer layers of epitaxial cerium oxide on sapphire obtained in this study can be used to create a master mask representing „islands" of epitaxial cerium oxide on sapphire. This result is planned to be used for fabrication of superconducting structures with submicron sizes.

Conflict of interest

The authors declare that they have no conflict of interest.

References

[1] Yu. Divin. Appl. Sci. **13**, 9, 5766 (2023).

[2] S. Benz, C. Hamilton. Appl. Phys. Lett. **68**, 22, 3171 (1996).

[3] A. Klushin, W. Prusseit, E. Sodtke, S.I. Borovitskii, L.E. Amatuni, H. Kohlstedt. Appl. Phys. Lett. **69**, 11, 1634 (1996).

[4] T. Schwarz, R. Wölbing, C.F. Reiche, B. Müller, M.J. Martínez-Pérez, T. Mühl, B. Büchner, R. Kleiner, D. Koelle. Phys. Rev. Appl. **3**, 4, 044011 (2015).

[5] C.H. Wu, Y.T. Chou, W.C. Kuo, J.H. Chen, L.M. Wang, J.C. Chen, K.L. Chen, U.C. Sou, H.C. Yang, J.T. Jeng. Nanotechnol. **19**, 31, 315304 (2008).

[6] A. Sosso, D. Andreone, V. Lacquaniti, A.M. Klushin, M. He, N. Klein. IEEE Trans. Appl. Supercond. **17**, 2, 874 (2007).

[7] L.S. Revin, D.V. Masterov, A.E. Parafin, S.A. Pavlov, D.A. Pimanov, A.V. Chiginev, A.V. Blagodatkin, I.V. Rakut', E.V. Skorokhodov, A.V. Gordeeva, A.L. Pankratov. Appl. Sci. **12**, 23, 11960 (2022).

[8] L.S. Revin, D.A. Pimanov, A.V. Chiginev, A.V. Blagodatkin, V.O. Zbrozhek, A.V. Samartsev, A.N. Orlova, D.V. Masterov, A.E. Parafin, V.Yu. Safonova, A.V. Gordeeva, A.L. Pankratov, L.S. Kuzmin, A.S. Sidorenko, S. Masi, P. de Bernardis. Beilstein J. Nanotechnol. **15**, 26 (2024).

[9] E.A. Matrozova, D.V. Masters, S.A. Pavlov, A.E. Parafin, L.S. Revin. Zhurnal radioelektroniki (elektron. zhurnal), **12**, 1 (2022). (in Russian).

[10] E.I. Glushkov, A.V. Chiginev, L.S. Kuzmin, L.S. Revin. Beilstein J. Nanotechnol. **13**, 325 (2022).

[11] O. Volkov, V. Pavlovskiy, I. Gundareva, R. Khabibullin, Y. Divin. IEEE Trans. Terahertz Sci. Technol. **11**, 3, 330 (2021).

[12] V.V. Pavlovskiy, I.I. Gundareva, O.Y. Volkov, Y.Y. Divin. Appl. Phys. Lett. **116**, 8, 082601 (2020).

[13] T. Zhang, J. Du, Y.J. Guo. IEEE J. Microwaves **2**, 3, 374 (2022).

[14] A. Sharafiev, M. Malnou, C. Feuillet-Palma, C. Ulysse, T. Wolf, F. Couedo, P. Febvre, J. Lesueur, N. Bergeal. Supercond. Sci. Technol. **31**, 3, 035003 (2018).

[15] S. Aghabagheri, M. Rasti, M.R. Mohammadizadeh, P. Kameli, H. Salamati, K. Mohammadpour-Aghdam, R. Faraji-Dana. Physica C **549**, 22 (2018).

[16] S. Ariyoshi, H. Mikami, A. Ebata, S. Ohnishi, T. Hizawa, S. Tanaka, K. Nakajima. Mater. Res. Express **8**, 11, 116001 (2021).

[17] I.K. Okakwu, P.E. Orukpe, E.A. Ogujor. Eur. J. Eng. Technol. Res. **3**, 7, 28 (2018).

[18] M. Malnou, C. Feuillet-Palma, C. Ulysse, G. Faini, P. Febvre, M. Sirena, L. Olanier, J. Lesueur, N. Bergeal. J. Appl. Phys. **116**, 7, 074505 (2014).

[19] J.V. Oboňa, S. Chromik, M. Spanková, Z. Öszi, I. Kostič. Physica C **435**, 1−2, 37 (2006).

[20] J.D. Pedarnig, M.A. Bodea, B. Steiger, W. Markowitsch, W. Lang. Phys. Procedia **36**, 508 (2012).

[21] W. Lang, M. Marksteiner, M. A. Bodea, K. Siraj, J.D. Pedarnig, R. Kolarova, P. Bauer, K. Haselgrübler, C. Hasenfuss, I. Beinik, C. Teichert. Nucl. Instrum. Meth. Phys. Res. B **272**, 300 (2012).

[22] V.K. Vasiliev, D.S. Korolev, S.A. Korolev, D.V. Masterov, A.N. Mikhaylov, A.I. Okhapkin, S.A. Pavlov, A.E. Parafin, P.A. Yunin, E.V. Skorokhodov, D.I. Tetelbaum. J. Surface Investigation: X-Ray, Synchrotron. Neutron Techniques **10**, *2*, 438 (2016).

[23] P.B. Mozhaev, G.A. Ovsyannikov, Y.L. Skov. ZhTF **69**, *2*, 119 (1999). (in Russian).

[24] S. Bevilacqua, S. Cherednichenco. IEEE Trans. Terahertz Sci. Technol. **4**, *6*, 653 (2014).

[25] D.V. Masterov, S.A. Pavlov, A.E. Parafin. Phys. Solid State **64**, *9*, 1172 (2022).

[26] Yu.N. Drozdov, S.A. Pavlov, A.E. Parafin. Pisma v ZhTF **24**, *1*, 55 (1998). (in Russian).

[27] J.R. Gavaler, J. Talvaccio, R.W. Weinert. IEEE Trans. Appl. Supercond. **5**, *2*, 1173 (1995).

Translated by A.Akhtyamov